Inorganic Chemistry

Article

pubs.acs.org/IC

Synthesis and Characterization of the Crystal Structure and Magnetic Properties of the New Fluorophosphate LiNaCo[PO_4]F

Hamdi Ben Yahia,*[,†] Masahiro Shikano,*[,†] Shinji Koike,[†] Kuniaki Tatsumi,[†] Hironori Kobayashi,[†] Hitoshi Kawaji,[‡] Maxim Avdeev,[§] Wojciech Miiller,[∥,§] Chris D. Ling,[∥] Jia Liu,[⊥] and Myung-Hwan Whangbo[⊥]

[†]Research Institute for Ubiquitous Energy Devices, National Institute of Advanced Industrial Science and Technology (AIST), Midorigaoka 1-8-31, Ikeda, Osaka 563-8577, Japan

[‡]Materials and Structures Laboratory, Tokyo Institute of Technology, 4259 Nagatsuta, Midori-ku, Yokohama-City, Kanagawa 226-8503, Japan

[§]Bragg Institute, B87, Australian Nuclear Science and Technology Organisation, Locked Bag 2001, Kirrawee DC NSW 2232, Australia

[∥]School of Chemistry, The University of Sydney, Sydney, NSW 2006, Australia

[⊥]Department of Chemistry, North Carolina State University, Raleigh, North Carolina 27695-8204, United States

Supporting Information

ABSTRACT: The new compound LiNaCo[PO_4]F was synthesized by a solid state reaction route, and its crystal structure was determined by single-crystal X-ray diffraction measurements. The magnetic properties of LiNaCo[PO_4]F were characterized by magnetic susceptibility, specific heat, and neutron powder diffraction measurements and also by density functional calculations. LiNaCo[PO_4]F crystallizes with orthorhombic symmetry, space group *Pnma*, with a = 10.9334(6), b = 6.2934(11), c = 11.3556(10) Å, and Z = 8. The structure consists of edge-sharing CoO_4F_2 octahedra forming $CoFO_3$ chains running along the b axis. These chains are interlinked by PO_4 tetrahedra forming a three-dimensional framework with the tunnels and the cavities filled by the well-ordered sodium and lithium atoms, respectively. The magnetic susceptibility follows the Curie–Weiss behavior above 60 K with $\theta = -21$ K. The specific heat and magnetization measurements show that LiNaCo[PO_4]F undergoes a three-dimensional magnetic ordering at T_{mag} = 10.2(5) K. The neutron powder diffraction measurements at 3 K show that the spins in each $CoFO_3$ chain along the b-direction are ferromagnetically coupled, while these FM chains are antiferromagnetically coupled along the a-direction but have a noncollinear arrangement along the c-direction. The noncollinear spin arrangement implies the presence of spin conflict along the c-direction. The observed magnetic structures are well explained by the spin exchange constants determined from density functional calculations.

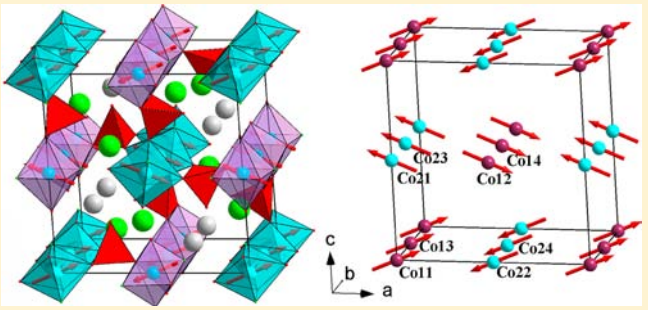

1. INTRODUCTION

The olivine phases LiMPO_4 (M: Mn, Fe, Co, Ni, Mg) have been extensively studied as positive electrode materials in lithium ion batteries. LiFePO_4 (theoretical capacity = 170 mAh/g) is a particularly promising example due to its advantages of being environmentally benign, inexpensive, and safe. LiFePO_4 is now commercialized as the active cathode element of a new generation of lithium-ion batteries. The performance of these batteries depends strongly on the electronic structure and the magnetic properties of these materials, which are very sensitive to the presence of impurities or defects.[1]

Since there is a need for a higher energy density, different attempts have been made to expand the capacity by using materials such as Li_2FeSiO_4 (theoretical capacity = 331 mAh/g), which theoretically could extract two lithium atoms per formula unit.[2] Another phase of interest in this regards is the A_2M[PO_4]F fluorophosphates (A: Li, Na and M: Mn, Fe, Co, Ni, Mg). Okada et al. have studied Li_2Co[PO_4]F and Li_2Ni[PO_4]F (theoretical capacity ≈ 287 mAh/g).[3,4] Intercalation of lithium into LiFe[PO_4]F leads to Li_2Fe[PO_4]F, which crystallizes in the Tavorite structure.[5,6] Nazar et al. also synthesized $Na_{2-x}Li_xM$[PO_4]F by different ion exchange methods starting from a layered structure of Na_2M[PO_4]F (M: Fe, Co, Mg) to find that these materials are promising as positive electrode materials for Li-ion or Na-ion energy storage devices.[7,8]

Although the electrochemical performances of these fluorophosphates have been intensively studied, there has been no report on the electronic and magnetic structure of these materials to our knowledge. Furthermore, their structures

Received: February 19, 2012
Published: August 2, 2012

   dx.doi.org/10.1021/ic300374w | *Inorg. Chem.* 2012, 51, 8729–8738

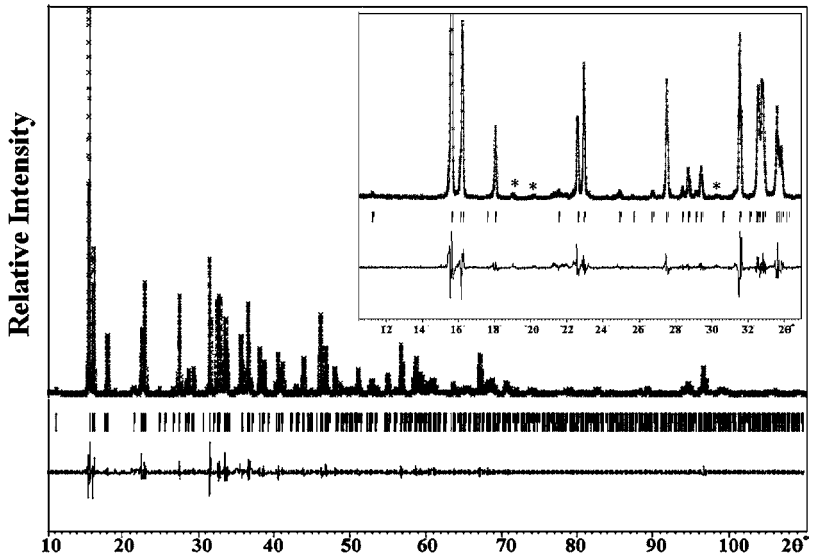

Figure 1. Final observed, calculated, and difference plots for XRPD (Cu−$K_{\alpha1,\alpha2}$ radiation) refinement of $LiNaCo[PO_4]F$.

have not been well characterized. For example, $Na_2Ni[PO_4]F$ was suggested to be isostructural with $Na_2Fe[PO_4]F$,[8] but we demonstrated recently that $Na_2Ni[PO_4]F$ has a new structure different from $Na_2M[PO_4]F$ (*M*: Fe, Co, Mg).[9] It is worthwhile to mention that $Li_2M[PO_4]F$ (*M*: Co, Ni) exhibits a 3D structure in which the transition metal atoms form infinite chains of edge sharing octahedra, whereas $Na_2M[PO_4]F$ (*M*: Fe, Co, Ni, Mg) possesses a layered structure with the transition metal atoms forming infinite chains made up of face-sharing octahedral dimer units.[9] Due to this structural difference, it is worth comparing the magnetic behaviors of these compounds. In addition, it is necessary to understand the influence of the size of the alkali metal on the structural changes within the $A_2M[PO_4]F$ fluorophosphates. This would help better design new materials for Li or Na batteries. For this goal, we started systematic studies on the crystal/electronic-structures and the magnetic/electrochemical properties of the intermediate phases $LiNaM[PO_4]F$ (*M* = Fe, Co, Ni).[9,10]

In the present work we synthesized a new compound $LiNaCo[PO_4]F$, solved the crystal structure by single crystal X-ray diffraction (XRD), and characterized its electrochemical properties. We also characterized $LiNaCo[PO_4]F$ by powder neutron diffraction, magnetic susceptibility, specific heat capacity measurements, and also by density functional theory (DFT) calculations.

2. EXPERIMENTAL SECTION

2.1. Synthesis. Powder samples of $LiNaCo[PO_4]F$ were prepared by direct solid state reaction from stoichiometric mixtures of LiF and $NaCoPO_4$ ($NaCoPO_4$ was obtained by heating a 1:2:2 mixture of Na_2CO_3, $(CH_3COO)_2Co{\cdot}4H_2O$, and $(NH_4)H_2PO_4$ at 350 °C for 6 h and at 750 °C for 12 h). The mixtures were ground in an agate mortar, pelletized, and heated at 700 °C for 12 h in a platinum crucible under air. The resulting powders were ground and fired at 700 °C for several days with intermediate grinding. The progress of the reactions was followed by powder XRD and a negligible amount of impurity was observed. The crystal used for the single crystal investigation was grown in a LiF/NaF flux. 100 mg of $LiNaCo[PO_4]F$ sample was thoroughly mixed in an agate mortar with 900 mg of LiF/NaF. The mixture was placed in a platinum tube and fired at 700 °C for 48 h and then cooled to room temperature at a rate of 15 °C/h. After washing the mixture with distilled water, pink, purple, white, and black single crystals of $LiNaCo[PO_4]F$, $Na_2Co[PO_4]F$, Li_3PO_4 and Co_3O_4, respectively were identified in the sample using the combination of EDX and single crystal diffraction analyses.

2.2. Electron Microprobe Analysis. Semiquantitative EDX analyses of different single crystals, including the ones investigated on the diffractometer, were carried out with a JSM-500LV(JEOL) scanning electron microscope. The experimentally observed compositions were close to the ideal one, $LiNaCo[PO_4]F$. Some crystals showed surface impurities of $Na_2Co[PO_4]F$, Li_3PO_4, or Co_3O_4. The resolution of the machine did not allow for a reliable determination of the lithium and oxygen content.

2.3. X-ray Diffraction. To ensure the purity of $LiNaCo[PO_4]F$ powder, high precision powder XRD measurements were performed. The data were collected at room temperature over the 2θ angle range of $10° \leq 2\theta \leq 110°$ with a step size of 0.005° using a Rigaku diffractometer operating with Cu$K\alpha1,\alpha2$ radiations. Full pattern matching refinements were performed with the JANA2006 program package (Figure 1).[11] The background was estimated by a Legendre function, and the peak shapes were described by a pseudo-Voigt function. The refinement of peak asymmetry was performed using four Berar-Baldinozzi parameters. Evaluation of these data revealed the refined cell parameters a = 10.9311(1), b = 6.28793(6), c = 11.3475(1) Å, and V = 779.95(1) Å ^{3}, in good agreement with the single crystal data listed in Table1.

Single crystals of $LiNaCo[PO_4]F$ suitable for XRD were selected on the basis of the size and the sharpness of the diffraction spots. The data collection was carried out on a Rigaku R-AXIS RAPID diffractometer using MoK_α radiation. Data processing and all refinements were performed with the JANA2006 program package. A spherical-type absorption correction was applied. For details of data collection, see Table 1.

2.4. Magnetic Susceptibility and Specific Heat Measurements. Magnetic susceptibility measurements of $LiNaCo[PO_4]F$ were carried out with a Quantum Design SQUID magnetometer. The susceptibility was recorded in the zero field cooled (ZFC) and field cooled (FC) modes, in the temperature range 2−310 K, with several applied external magnetic fields H. For the measurement of time-dependent remnant magnetization, the sample was zero-field-cooled from 50 to 2 K. A magnetic field of 2 T was then applied for 10 min before being switched off. The time at which the field was set to zero is taken as t = 0, and the decay of magnetization was recorded as a function of time. Heat capacity measurements were performed on $LiNaCo[PO_4]F$ pellet using a PPMS Quantum Design in a temperature range from 2 to 310 K.

2.5. Neutron Powder Diffraction. Neutron powder diffraction (NPD) data were collected on the high-resolution diffractometer Echidna at the OPAL facility (Lucas Height, Australia) using neutrons

dx.doi.org/10.1021/ic300374w | Inorg. Chem. 2012, 51, 8729−8738

Table 1. Crystallographic Data and Structure Refinement for $LiNaCo[PO_4]F$

parameter	value or remarks
formula	$LiNaCo[PO_4]F$
crystal color	pink sphere
crystal radius mm	0.050
M, g mol^{-1}	202.8
crystal system	orthorhombic
space group	*Pnma*
a, Å	10.9334 (6)
b, Å	6.2934(11)
c, Å	11.3556(10)
V, Å^3	781.36(16)
Z	8
density calcd., g cm^{-3}	3.45
temperature, K	293 (1)
$F(000)$, e	776
diffractometer	Rigaku R-AXIS RAPID
monochromator	graphite
radiation	MoK_α, 0.71069 Å
scan mode	multiscan
h k l range	$-14 < h < 12$
	$-8 < k < 8$
	$-14 < l < 14$
θ_{min}, θ_{max}, deg	3.59, 27.46
linear absorption coeff., mm^{-1}	4.83
absorption correction	sphere
T_{min}/T_{max}	0.4932/0.5009
no. of reflections	6383
no. of independent reflections	969
reflections used $[I \geq 2\sigma(I)]$	752
R_{int}	0.045
refinement	F^2
no. of refined parameters	100
R factors $R(F)/wR(F^2)$	0.0282/0.0651
g. o. f.	1.11
weighting scheme	$w = 1/(\sigma^2(I) + 0.0009I^2)$
diff. Fourier residues, e$^-$ Å^{-3}	−0.42/+0.46

of wavelength 2.4395 Å. For the measurements the sample in the form of ∼2 g of powder was loaded in a 6 mm diameter cylindrical vanadium can, and the data were collected at 300 K and 3 K using a closed-cycle refrigerator. The Rietveld analysis of the data was performed using the Fullprof Suite[12] with the default neutron scattering lengths and Co^{2+} magnetic form-factors.

2.6. Density Functional Analysis of Magnetic Structure. In our study of the magnetic structure of $LiNaCo[PO_4]F$, we carried out spin-polarized density functional calculations using the projector augmented wave method implemented in the Vienna *ab initio* simulation package[13] with the generalized gradient approximation (GGA)[14] for the exchange-correlation functional, the plane-wave cutoff energy of 400 eV, a set of 45 k-points for the irreducible Brillouin zone, and the threshold 10^{-6} eV for energy convergence. To examine the possible effect of the electron correlation associated with Co 4d states, we carried out GGA plus on-site repulsion U (GGA+U) calculations[15] with the effective U = 1, 2, 3, and 4 eV on the Co atoms. Our spin polarized GGA+U calculations for the ferromagnetic state of the orbital-ordered structure of $LiNaCo[PO_4]F$ show a band gap even when U = 1 eV, and the band gap increases with increasing the U value.

2.7. Electrochemical Cycling. Positive electrodes were made from mixtures of $LiNaCo[PO_4]F$ or $LiNaCo_{1/2}Fe_{1/2}[PO_4]F$ powder, acetylene black (AB), and polyvinylidene fluoride (PVDF) binder dissolved in N-methylpyrrolidone in a weight ratio of 70:22:8. The obtained slurry was mixed for 1 h and coated onto an Al foil. The resulting electrode films were pressed with a twin roller, cut into a round plate (14 mm in diameter), and dried at 110 °C for 12 h under vacuum. $LiNaCo[PO_4]F$ or $LiNaCo_{1/2}Fe_{1/2}[PO_4]F$/$LiPF_6$+EC +DMC/Li coin-type cells (CR2032) were assembled, in an argon-filled glovebox, with polypropylene as separator. CC−CV testing was performed using BTS2003H (Nagano Co., Ltd.) battery tester system in a potential range of 1.0−5.0 V at a rate of C/5 (that is, one lithium per formula unit in 5 h).

3. RESULTS AND DISCUSSION

3.1. Structure Refinement. The extinction conditions observed for $LiNaCo[PO_4]F$ were compatible with the space group *Pnma and* $Pna2_1$. The structure was solved in the centrosymmetric group *Pnma*. Most of the atomic positions were located using the superflip program implemented in the JANA2006 package. The use of difference-Fourier synthesis allowed us to localize the remaining oxygen atom positions. The bond valence analysis enabled us to distinguish between the O^{2-} and F^- anions. With anisotropic displacement parameters for all positions, the residual factors converged to the values listed in Table 1. Inspection of the databases revealed the structural relationship with $Li_2Ni[PO_4]F$,[16] $Li_2Co[PO_4]F$,[5] and $Li_{2.32}Fe^{3+}_{0.56}[PO_4]F$.[17] The refined atomic positions and anisotropic displacement parameters (ADPs) are given in

Table 2. Atom Positions and Isotopic Displacement Parameters (Å^2) for $LiNaCo[PO_4]F$

atom		x	y	z	U_{eq} (Å^2)
Co1	4*a*	0	0	0	0.00965(19)
Co2	4*b*	0	0	1/2	0.00975(19)
P1	4*c*	0.04193(11)	1/4	0.74266(10)	0.0098(3)
P2	4*c*	0.24660(9)	1/4	0.07828(11)	0.0093(3)
Na1	8*d*	0.22335(13)	0.00825(19)	0.34659(12)	0.0203(4)
Li2	4*c*	0.2738(7)	1/4	0.5903(6)	0.013(2)
Li3	4*c*	−0.0506(7)	1/4	0.2676(7)	0.015(2)
O1	8*d*	0.18045(18)	0.0490(3)	0.03573(19)	0.0131(6)
O2	4*c*	0.2659(3)	1/4	0.2096(3)	0.0150(10)
O3	4*c*	0.1814(3)	1/4	0.7418(3)	0.0139(10)
O4	4*c*	0.3752(3)	1/4	0.0164(3)	0.0130(9)
O5	4*c*	0.4921(2)	1/4	0.6288(3)	0.0120(9)
O6	8*d*	0.00739(19)	0.5483(3)	0.31988(19)	0.0116(6)
F1	4*c*	0.1276(2)	1/4	0.4731(2)	0.0140(8)
F2	4*c*	0.4410(2)	1/4	0.3935(2)	0.0158(8)

dx.doi.org/10.1021/ic300374w | *Inorg. Chem.* 2012, 51, 8729−8738

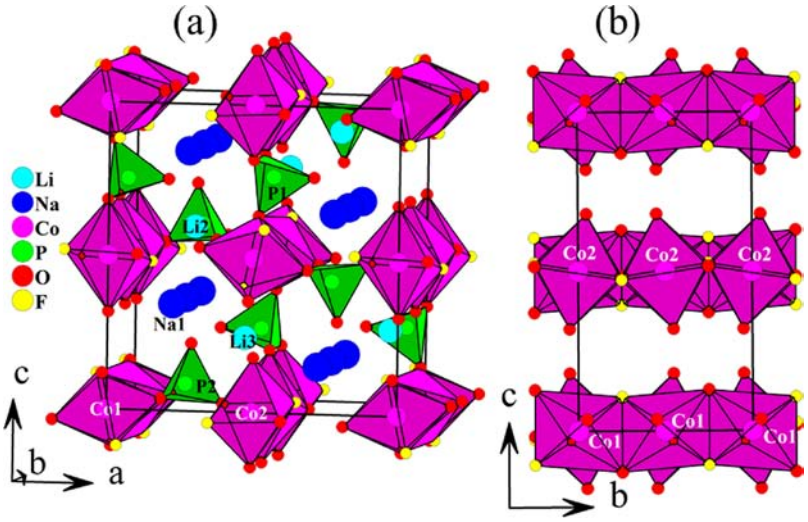

Figure 2. Perspective view of the $LiNaCo[PO_4]F$ structure (a) and view along [100] (b) without the phosphorus and alkali metal atoms for clarity reasons.

Table 3. Interatomic Distances (in Å) and Bond Valences (B.V.) for $LiNaCo[PO_4]F$[b]

	distance	B.V.		distance	B.V.
Na1−O2	2.225(3)	0.320	Co1−O1 (×2)	2.038(2)	0.393 (×2)
Na1−O3	2.268(2)	0.285	Co1−F2 (×2)	2.0864(16)	0.307 (×2)
Na1−F1	2.340(2)	0.167	Co1−O5 (×2)	2.150(2)	0.290 (×2)
Na1−O6	2.407(2)	0.195	<Co1−X>	2.0914	1.980[a]
Na1−O1	2.419(3)	0.189			
Na1−O4	2.742(3)	0.079	Co2−O6 (×2)	2.069(2)	0.361 (×2)
Na1−F2	2.874(3)	0.039	Co2−O4 (×2)	2.0911(19)	0.340 (×2)
		1.156[a] [C.N. = 5]	Co2−F1 (×2)	2.1246(17)	0.277 (×2)
		1.274[a] [C.N. = 7]	<Co2−X>	2.0949	1.956[a]
Li2−O3	1.995(8)	0.239	P1−O3	1.525(3)	1.282
Li2−O1 (×2)	2.043(4)	0.210 (×2)	P1−O6 (×2)	1.551(2)	1.195 (×2)
Li2−F1	2.081(8)	0.142	P1−O5	1.559(3)	1.170
Li2−O5	2.426(8)	0.075		<1.5465>	4.842[a]
Li2−F2	2.887(8)	0.016			
		0.801[a] [C.N. = 4]	P2−O2	1.506(4)	1.350
		0.876[a] [C.N. = 5]	P2−O1 (×2)	1.535(2)	1.248 (×2)
		0.892[a] [C.N. = 6]	P2−O4	1.572(3)	1.129
				<1.537>	4.975[a]
Li3−F2	1.832(8)	0.279			
Li3−O2	2.022(8)	0.223			
Li3−O6 (×2)	2.068(4)	0.197 (×2)			
Li3−O4	2.584(8)	0.049			
		0.896[a] [C.N. = 4]			
		0.945[a] [C.N. = 5]			

[a]Bond valence sum, B.V. = $e^{(r0-r)/b}$ with the following parameters: b = 0.37, r_0 (Na^I−O) = 1.803, r_0 (Na^I−F) = 1.677, r_0 (Li^I−O) = 1.466, r_0 (Li^I−F) = 1.360, r_0 (Co^{II}−O) = 1.692, r_0 (Co^{II}−F) = 1.649 and r_0 (P^V−O) = 1.617 Å.[18,19] [b]Average distances are given in brackets.

Tables 2 and S1, respectively. Further details on the structure refinement may be obtained from the Fachinformationszentrum Karlsruhe, D-76344 Eggenstein-Leopoldshafen (Germany), by quoting the Registry No. CSD-424194.

3.2. Crystal Structure. $LiNaCo[PO_4]F$ is isostructural with $Li_2Ni[PO_4]F$.[16] The structure consists of edge-sharing chains of CoF_2O_4 octahedra running along the b axis (Figures 2a, b). The $CoFO_3$ infinite chains are cross connected by the PO_4 tetrahedra, giving rise to channels and cavities in which the sodium and the lithium atoms are located, respectively (Figure 2a). Interatomic distances and bond valence sums (BVSs)[18,19] are listed in Table 3.

In the $Co1F_2O_4$ octahedra, the Co1−X distances range from 2.038 to 2.150 Å with an average value of 2.091 Å, whereas in the $Co2F_2O_4$ octahedra the Co2−X distances range from 2.069 to 2.125 Å with an average distance of 2.095 Å. Such a six-coordinate Co^{2+} environment occurs also in $Ba_2Co[CO_3]_2F_2$[20] with distances ranging from 2.046 to 2.111 Å and an average distance of 2.073 Å, in good agreement with our results. The BVSs of 1.980 and 1.956 are in very good agreement with the expected value of +2 for Co^{2+}. It is noted that the $Co1F_2O_4$ octahedron [Co1−O = 2.038 (×2), 2.145 (×2), and Co1−F = 2.087 (×2) Å] is described as an axially elongated CoF_2O_4 octahedron with axially elongated Co−O bonds, but $Co2F_2O_4$

dx.doi.org/10.1021/ic300374w | Inorg. Chem. 2012, 51, 8729−8738

octahedron [Co2−O = 2.069 (×2), 2.091 (×2), and Co2−F = 2.125 (×2) Å] as an axially elongated CoF_2O_4 octahedron with axially elongated Co−F bonds.

The $P1O_4$ tetrahedron is quite regular, however, $P2O_4$ is slightly distorted with one short and one stretched P−O distances of 1.506 and 1.572 Å, respectively. The average P−O distances of 1.546 and 1.537 Å for P1 and P2, respectively, are consistent with the value of 1.55 Å estimated from the effective ionic radii of the four-coordinated P^{5+} and O^{2-}.[21] The BVSs of 4.84 and 4.97 are in agreement with the expected value of +5 for P^{5+}.

The Na^+ ion is bonded to four O^{2-} and one F^- atoms to form a distorted square pyramid (Figure 3a). Such coordination is similar to that of Li1 in the $Li_2Ni[PO_4]F$. The average Na−X distance is 2.332 Å. The BVS calculation by using the five shortest Na−X contacts shows that Na1 is overbonded with a value of 1.156.

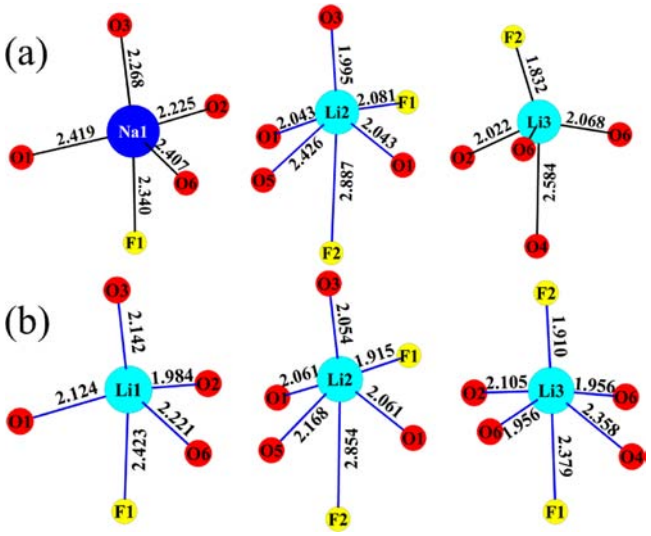

Figure 3. Surrounding of the sodium and lithium atoms in $LiNaCo[PO_4]F$ (a) and $Li_2Ni[PO_4]F$ structures (b).

The coordination polyhedra of the Li ions are not well-defined. If one considers only the shortest Li−X distances, both Li2 and Li3 would be tetrahedral coordinated. However, the BVS calculations show that both Li atoms are strongly underbonded. When the coordination sphere of Li2 and Li3 are increased to five (Figure 3a), the BVSs become 0.876 and 0.945, respectively. Thus, the Li2 and Li3 atoms are best considered to be 4 + 1 coordinate (see the Li−X distances listed in Table 3). The Li2 square pyramid is strongly distorted compared with the environment of Li2 in the $Li_2Ni[PO_4]F$ (Figure 3a, 3b). The Li3 environments of $LiNaCo[PO_4]F$ and $Li_2Ni[PO_4]F$ are also different, namely, they are distorted square pyramid and octahedron, respectively.

The crystal structures of $LiNaCo[PO_4]F$, $CuMnVO_4$,[22] and $NaMnVO_4$[23] are slightly similar. Indeed, in these three different structures, the $Li_2Ni[PO_4]F$, the Na_2CrO_4- and the maricite-types, respectively, infinite chains made up of edge-sharing MX_6 (M = Ni, Cr, Mn) octahedra are interlinked by PO_4 or VO_4 tetrahedra. As $NaMnVO_4$ and α-$NaCoPO_4$[24] have the same structure, the maricite type structure, and since α-$NaCoPO_4$ + LiF = $LiNaCo[PO_4]F$, one could expect the possible formation of $LiNaMn[VO_4]F$ by mixing $NaMnVO_4$ with LiF (this will be conducted in the near future).

The replacement of Li by Na atoms in $Li_2Co[PO_4]F$ is expected to induce a strong distortion of the $Co2F_2O_4$ octahedra. Indeed, since Na is bigger than Li, octahedra tilts around the *a* axis are expected (Figure 4a). This would induce face-sharing instead of edge-sharing octahedra (Figure 4b). This is most probably at the origin of the structural transition from $Li_2Co[PO_4]F$- to $Na_2Co[PO_4]F$-type in which the $Co2F_2O_4$ octahedra share faces (Figure 4c). This structural transition is accompanied by a new distribution of the cations and anions.[25]

3.3. Magnetic Susceptibility and Specific Heat Measurements of $LiNaCo[PO_4]F$. The magnetic susceptibility χ vs T and the corresponding χ^{-1} vs T for $LiNaCo[PO_4]F$ are shown in Figure 5. The χ^{-1} vs T plot reveals that $LiNaCo[PO_4]F$ exhibits a paramagnetic behavior in the temperature range 60−310 K. The susceptibility above 60 K follows a Curie−Weiss law with θ = −21 K and C = 3.16 $mol^{-1}{\cdot}cm^3{\cdot}K$. The negative θ indicates that the predominant spin exchange interactions are AFM. The effective magnetic moment μ_{eff} calculated from the Curie constant 5.03 μ_B is a typical value obtained for divalent cobalt atoms, although higher than the spin only value of 3.87 μ_B expected for a high-spin Co^{2+} (d^7) ion. This is due to contribution from the orbital angular momentum.

In addition, magnetic magnetization measured as a function of temperature under magnetic field H of 25 and 1500 Oe revealed the divergence between the ZFC and FC susceptibility at ∼11 K (Figure 6). This anomaly points to a ferromagnetic-like response, with magnetization increasing rapidly below T_{mag}.

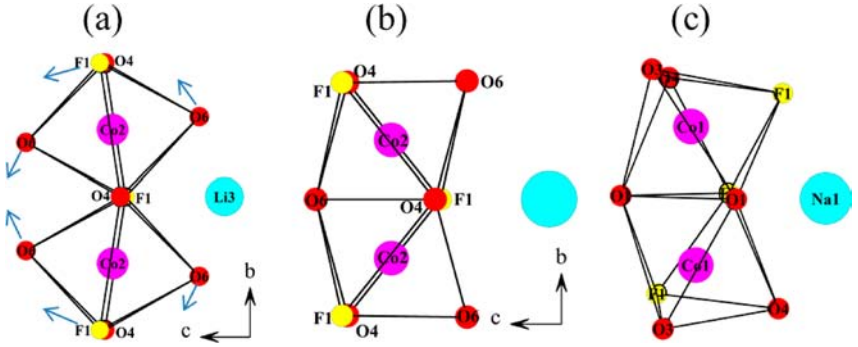

Figure 4. (a) View of $Co2O_4F_2$ octahedra sharing edges in $LiNaCo[PO_4]F$, (b) theoretical tilting of the CoO_4F_2 octahedra induced by the replacement of the lithium by a bigger atom, and (c) view of $Co1O_4F_2$ octahedra sharing faces in $Na_2Co[PO_4]F$. The arrows indicate the rotation of the MO_4F_2 octahedra.

dx.doi.org/10.1021/ic300374w | Inorg. Chem. 2012, 51, 8729−8738

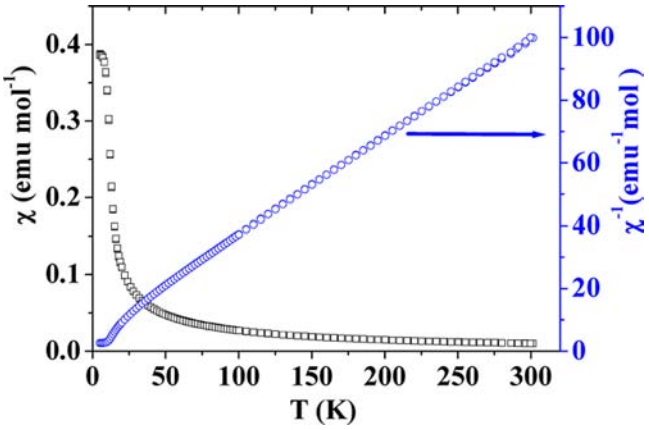

Figure 5. Magnetic susceptibility χ vs temperature and the corresponding χ^{-1} vs T plots of LiNaCo[PO_4]F measured with the applied field H = 10 kOe.

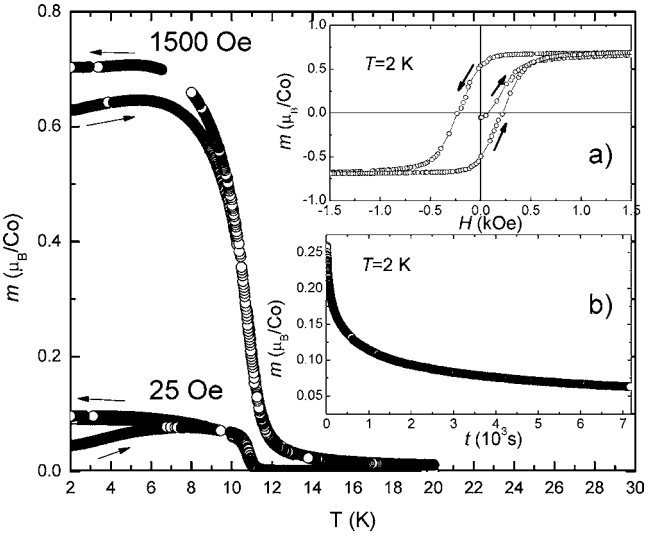

Figure 6. Magnetization of LiNaCo[PO_4]F collected at 25 and 1500 Oe magnetic field vs temperature. Left- and right-pointing arrows indicate FC and ZFC conditions, respectively. Insets show hysteresis loop (a) and magnetic relaxation (b) collected at T = 2 K.

Magnetization measured at 2 K as a function field showed opening of a hysteresis loop with remnant magnetization of 0.53 μ_B/Co and coercive field of 240 Oe (Figure 6, inset (a)). Although this also suggested a long-range ferromagnetic order, an extremely low coercive field may equally result in a field-induced magnetization typical for materials with short-range magnetic correlations, e.g. spin glasses. To test the latter scenario, we have performed a magnetic relaxation experiment, and the results are depicted in Figure 6, inset (b). The observed decay of remnant magnetic moment from about 0.25 to 0.06 μ_B/Co after 2 h points to a spin-glass character of ferromagnetic-like behavior.[26] As will be discussed later, such a magnetic behavior is consistent with the results of the NPD data analysis which revealed a long-range antiferromagnetic order of the Co^{2+} magnetic moments with a small spin canting. Such an arrangement often results in complex coexistence of features typical for long- and short-range magnetic order as was observed in various frustrated magnetic systems.[27]

Figure 7 shows the temperature dependence of the specific heat capacity (C_p) and the specific heat divided by temperature

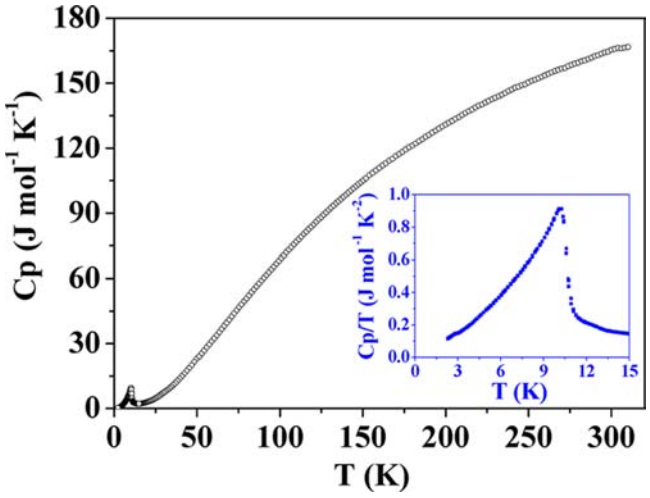

Figure 7. Heat capacities $Cp(T)$ of LiNaCo[PO_4]F. The inset displays Cp/T in the region of the phase transition at 10.2(5) K.

(C_p/T) for LiNaCo[PO_4]F. A λ anomaly indicating the long-range magnetic ordering of Co^{2+} ions is found at 10.2(5) K, which corresponds to the result of the magnetic susceptibility measurements.

3.4. Crystal and Magnetic Structure from Neutron Powder Diffraction Measurements. The Rietveld analysis of the neutron powder diffraction data collected at 300 K using as a starting model the structure solved from the X-ray single crystal diffraction data (see Section 3.2) resulted in good agreement between the experimental and calculated patterns (Figure S1 of the Supporting Information). The root-mean-square difference in the Cartesian coordinates of all the atoms between the X-ray single crystal and neutron powder diffraction models amounted to only 0.00572. Neutron diffraction is more sensitive to distribution of lithium in a crystal structure and especially to the Na/Li mixing, if any, than XRD due to high contrast in neutron scattering lengths of sodium and lithium (3.63 and −1.90 fm, respectively). However, we did not find any statistically significant Na/Li disorder during the analysis of the neutron powder diffraction data. The crystallographic data for LiNaCo[PO_4]F based on the analysis of the NPD data are listed in Table S2 of the Supporting Information.

Examination of the neutron diffraction data collected at 3 K compared to that collected at 300 K revealed additional diffraction peaks of presumably antiferromagnetic ordering origin consistent with the magnetic susceptibility data (Figure 8). All the diffraction peaks with magnetic contribution could be indexed by the crystallographic unit cell, i.e., with the propagation vector $\boldsymbol{k}$ = (0, 0, 0). For the 4a(0,0,0) and 4b(0,0,1/2) Wyckoff sites of the *Pnma* space group the magnetic representation decomposes in terms of one-dimensional irreducible representations (IR) as $\Gamma=3\Gamma_1+3\Gamma_3+3\Gamma_5+3\Gamma_7$. The associated basis vectors are listed in Table 4.

The best agreement between the experimental and calculated powder diffraction patterns was obtained for the Γ_7 (FxCyGz) representation with the Co1 and Co2 chains coupled antiferromagnetically. Further examination of the diffraction patterns revealed that the reflections corresponding to the C magnetic mode are absent, and therefore the associated basis function mixing coefficient was fixed to zero in the following refinements. The attempts to introduce a net moment to the model by making the Co1 and Co2 moments noncollinear

dx.doi.org/10.1021/ic300374w | Inorg. Chem. 2012, 51, 8729−8738

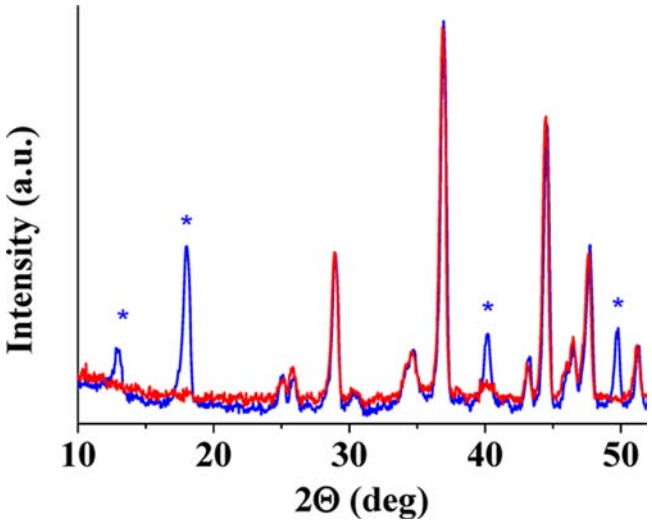

Figure 8. LiNaCo[PO_4]F neutron powder diffraction data collected at 3 K and 300 K. Additional peaks observed at low temperature are indicated with star symbols.

Table 4. Basis Vectors for the 4*a*(0,0,0) and 4*b*(0,0,1/2) Sites of the *Pnma* Space Group and the Propagation Vector *k* = (0,0,0)[a]

IR	basis vectors	Shubnikov group
Γ_1	Ax Gy Cz	*Pnma*
Γ_3	Gx Ay Fz	*Pn′m′a*
Γ_5	Cx Fy Az	*Pn′ma′*
Γ_7	Fx Cy Gz	*Pnm′a′*

[a]The atomic positions are Co11 (0,0,0), Co12 (1/2,0,1/2), Co13 (0,1/2,0), Co14 (1/2,1/2,1/2), Co21(0,0,1/2), Co22(1/2,0,0), Co23-(0,1/2,1/2), and Co24(1/2,1/2,0), respectively. The ordering modes are F(+ + + +), C(+ + - -), G(+ - + -), and A(+ - - +).

along *a* axis in order to test whether a hysteresis loop observed at 2 K (Figure 6) is a manifestation of long-range ferrimagnetic order were unsuccessful. Regardless of the starting Co1 and Co2 magnetic moment directions the refinement converged to their antiparallel orientation within a few estimated standard deviations. Thus, we explain the ferromagnetic-like response observed below T_{mag} by a short-range spin-glass behavior likely related to local variation in spin canting angle. The explanation is supported by magnetic relaxation measurements (Figure 6, inset (b)). The final Rietveld plot is presented in Figure 9, and the magnetic structure is illustrated in Figure 10. The information on crystal structure is listed in Table S3 of the Supporting Information.

3.5. Spin Exchange Interactions and Magnetic Structure. The magnetic structure determined from neutron diffraction measurements shows that the spins in each $CoFO_3$ chain along the *b*-direction are ferromagnetically coupled, and these FM chains in the *ab*-planes are antiferromagnetically coupled along the *a*-direction. However, the FM chains in the *bc*-plane have a noncollinear arrangement (~136° between adjacent spin vectors) along the *c*-direction (Figure 10), which implies the presence of spin conflict along the *c*-direction. This is apparently surprising because the index of spin frustration $f = |\theta|/T_N \approx 2$ is rather small.[28]

To gain insight into the observed magnetic properties of LiNaCo[PO_4]F, we evaluate the eight spin exchange interactions, J_1, $J_{1'}$, J_2, $J_{2'}$, J_3, $J_{3'}$, J_4, and $J_{4'}$ defined in Figure

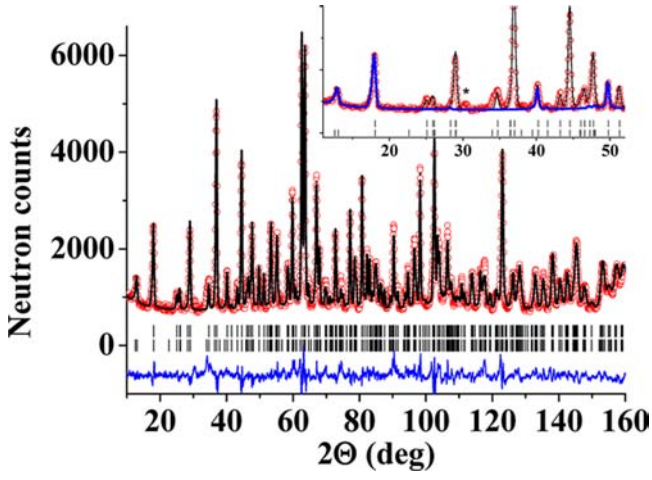

Figure 9. The Rietveld plot for LiNaCo[PO_4]F at 3 K: a = 10.8946(2) Å, b = 6.2652(1) Å, c = 11.3166(2) Å, V = 772.43(2) Å^3, R_p = 5.40%, R_{wp} = 7.10, R_{Bragg} = 7.92%, R_{mag} = 8.93%. The blue curve in the inset shows magnetic contribution. The star symbol indicates an impurity peak consistent with the Co_3O_4 diffraction data.

11 by performing energy-mapping analysis based on DFT electronic structure calculations.[29] We consider the nine ordered spin states shown in Figure 11 and determine their relative energies per eight FUs by performing GGA+U calculations with U = 1 and 2 eV (Table 5). Here the ground state (GS) refers to the observed magnetic structure, and our calculations show that the GS is indeed found to be the lowest energy state of the nine ordered spin states. The GS is not calculated to be the lowest-energy state for U = 3 eV or greater. In terms of the spin Hamiltonian, $\hat{H} = -\sum_{i<j} J_{ij}\hat{S}_i\cdot\hat{S}_j$, where J_{ij} is the spin exchange constant for the interaction between the sites i and j. Then, by using the expressions of the spin exchange interactions for spin dimers with N unpaired spins per site (N = 3 in the present case),[30] the total spin exchange energies, per eight FUs, of the nine ordered spin states are written as

$$\mathrm{FM} = -(4J_1 + 4J_{1'} + 8J_2 + 8J_{2'} + 16J_3 + 16J_{3'} + 8J_4 + 8J_{4'})(N^2/4)$$

$$\mathrm{AF1} = -(-4J_1 + 4J_{1'} + 8J_4 + 8J_{4'})(N^2/4)$$

$$\mathrm{AF2} = -(4J_1 - 4J_{1'} + 8J_4 + 8J_{4'})(N^2/4)$$

$$\mathrm{AF3} = -(-4J_1 - 4J_{1'} - 8J_2 + 8J_{2'} + 16J_3 - 16J_{3'} - 8J_4 - 8J_{4'})(N^2/4)$$

$$\mathrm{AF4} = -(-4J_1 - 4J_{1'} + 8J_2 + 8J_{2'} - 16J_3 - 16J_{3'} + 8J_4 + 8J_{4'})(N^2/4)$$

$$\mathrm{AF5} = -(-4J_1 - 4J_{1'} + 8J_2 - 8J_{2'} - 16J_3 + 16J_{3'} - 8J_4 - 8J_{4'})(N^2/4)$$

$$\mathrm{AF6} = -(8J_{2'})(N^2/4)$$

$$\mathrm{AF7} = -(4J_1 + 4J_{1'} + 8J_4 - 8J_{4'})(N^2/4)$$

$$\mathrm{GS} = -(4J_1 + 4J_{1'} - 8J_2 - 8J_{2'} - 16J_3 - 16J_{3'} + 8J_4 + 8J_{4'})(N^2/4)$$

dx.doi.org/10.1021/ic300374w | Inorg. Chem. 2012, 51, 8729−8738

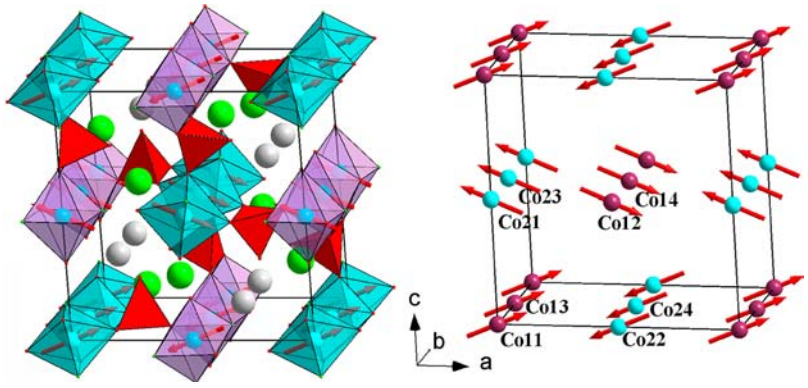

Figure 10. The magnetic structure of $LiNaCo[PO_4]F$ at 3 K. The components of the moment along *x*, *y*, and *z* axes are 2.13(2), 0, and 0.87(2) μ_B, respectively. The total moment is 2.30(2) μ_B, and the angle between the moment direction and the *ab*-plane is 22.2°.

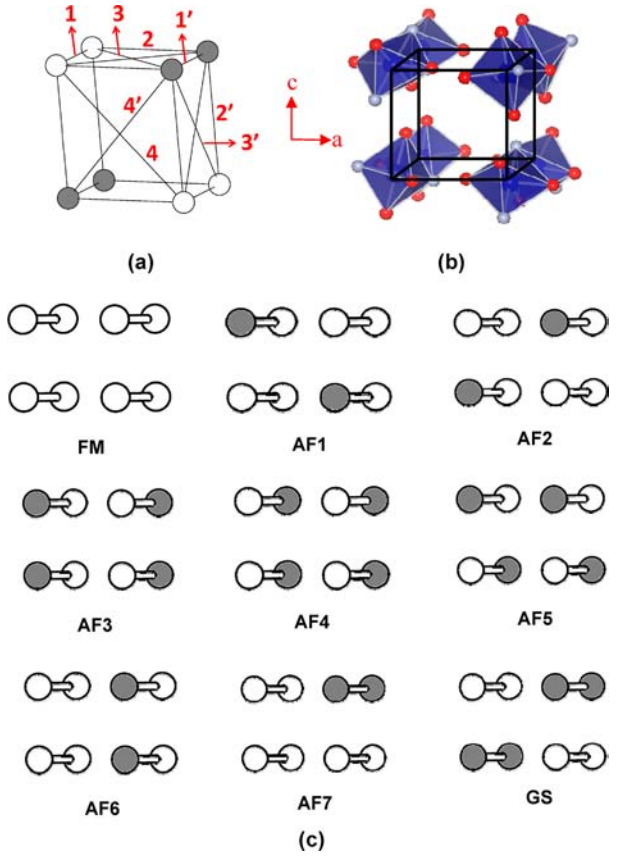

Figure 11. (a, b) Definitions of the spin exchange paths. The Co1 and Co2 atoms are indicated as empty and filled circles, respectively. The numbers 1, 2, 3, 4, 1′, 2′, 3′, and 4′ refer to the spin exchanges J_1, J_2, J_3, J_4, $J_{1'}$, $J_{2'}$, $J_{3'}$, and $J_{4'}$, respectively. (c) Nine ordered spin arrangements of the Co1 and Co2 spin sites used to extract the values of J_1, J_2, J_3, J_4, $J_{1'}$, $J_{2'}$, $J_{3'}$, and $J_{4'}$ by GGA+U calculations. The positions of the Co1FO3 and Co2FO3 chains are identical with those of (a, b), and the up-spin and down-spin Co^{2+} sites are indicated by empty and filled circles, respectively.

Then, by mapping the relative energies of the nine ordered spin states determined from GGA+U calculations onto the corresponding relative energies determined from the above expressions, we obtain the values of J_1−$J_{4'}$ listed in Table 6.

To check the proper range of *U* values, we calculate the Curie−Weiss temperature θ in the mean-field approximation by using the calculated spin exchange parameters.[31] Since there are two nonequivalent Co sites in the 50:50 ratio, θ can be written as

$$\theta = \frac{S(S+1)}{3k_B}\sum_{ii} z_i J_i$$

$$= \frac{S(S+1)}{3k_B}[0.5(2J_1 + 2J_2 + 2J_{2'} + 4J_3 + 4J_{3'} + 4J_4 + 4J_{4'}) + 0.5(2J_{1'} + 2J_2 + 2J_{2'} + 4J_3 + 4J_{3'} + 4J_4 + 4J_{4'})]$$

The θ determined by using the calculated *J* values are also listed in Table 6. The calculated θ is greater than the experimental value (−21 K) by a factor of 2−2.5. Thus, in our analysis of the experimental magnetic properties in terms of our calculated spin exchanges, it is necessary to consider the trends that are independent of the *U* values used to calculate them.

We now discuss the observed magnetic structure of $LiNaCo[PO_4]F$ on the basis of the calculated spin exchanges listed in Table 6. The dominant spin exchanges are $J_{1'}$, J_3. $J_{3'}$, J_4, and $J_{4'}$. Due to the strong FM exchange $J_{1'}$, the spins of each $Co2FO_3$ chain become ferromagnetically coupled. Because of the strong AFM interchain exchange J_3 and the weak intrachain exchange J_1, the spins of each $Co1FO_3$ chain also become ferromagnetically coupled. Along the *a*-direction, each FM $Co2FO_3$ chain becomes antiferromagnetically coupled with its adjacent FM $Co1FO_3$ chains due to the strong AFM exchange J_3. Now let us consider the noncollinear spin arrangement between the FM $CoFO_3$ chains along the *c*-direction. If only the interchain AFM exchange $J_{3'}$ is considered, an AFM arrangement between them would be predicted. However, the

Table 5. Relative Energies (in meV per Eight FUs) of the Nine Ordered Spin States of $LiNaCo[PO_4]F$ Determined from GGA +U Calculations with U = 1−2 eV

U (eV)	FM	AF1	AF2	AF3	AF4	AF5	AF6	AF7	GS
1	76.32	44.12	51.55	54.89	9.88	49.06	47.84	53.84	0
2	57.70	28.59	34.04	36.29	2.12	31.78	31.31	42.56	0

dx.doi.org/10.1021/ic300374w | *Inorg. Chem.* 2012, 51, 8729−8738

Table 6. Values of the Spin Exchange Constants (in K) of LiNaCo[PO_4]F Determined from GGA+U Calculations with U = 1−2 eV and the Curie−Weiss Temperature θ (in K) Obtained from the Calculated Spin Exchanges by Using the Mean Field Theory

U (eV)	J1	J1′	J2	J2′	J3	J3′	J4	J4′	θ/K
1	3.84	8.63	−1.79	4.84	−8.10	−5.73	−6.84	5.05	−50
2	−0.17	3.35	0.08	0.79	−4.68	−5.06	−4.34	4.42	−42

interchain FM exchange $J_{2'}$ is comparable in magnitude with the intrachain FM exchange $J_{1'}$. Thus, the ($J_{1'}$, $J_{2'}$, $J_{3'}$) triangles lead to spin conflict between adjacent FM $CoFO_3$ chains along the c-direction.[28] Consequently, the FM $CoFO_3$ chains adopt the noncollinear spin arrangement along the c-direction. In the (J_2, $J_{2'}$, J_4) and (J_2, $J_{2'}$, $J_{4'}$) triangles, the extent of spin conflict is negligible because J_2 is weak.

3.6. Electrochemical Properties. LiNaCo[PO_4]F shows an electrochemical activity above 5 V in the lithium cell. At this voltage most of the conventionally used electrolytes decompose. Therefore, to study accurately the electrochemical properties of this material, the development of stable electrolyte above 5 V is required. This work is still in progress and will be published in the future.

We have made several attempts to decrease the working potential by replacing cobalt by iron. Indeed when half of the cobalt is replaced by iron, the working potential decreases significantly, but still a stable electrolyte up to 5 V is required in order to extract at least one alkali metal atom. The discharge−charge curves of $LiNaCo_{1/2}Fe_{1/2}[PO_4]F$ are depicted in Figure S2.

4. CONCLUSIONS

The new compound LiNaCo[PO_4]F synthesized by a solid state reaction route consists of $CoFO_3$ chains made up of edge-sharing CoO_4F_2 octahedra along the b axis. The $CoFO_3$ chains along the b-direction are interlinked by PO_4 tetrahedra forming a three-dimensional framework. The magnetic susceptibility follows the Curie−Weiss behavior above 60 K with θ = −21 K. The magnetic susceptibility and the magnetization measurements show that LiNaCo[PO_4]F undergoes a 3D magnetic ordering at T_N = 10.2(5) K with additional spin-glass features. The ordered magnetic structure of LiNaCo[PO_4]F determined by neutron powder diffraction at 3 K shows that the spins in each $CoFO_3$ chain along the b-direction are ferromagnetically coupled, while such FM chains are antiferromagnetically coupled along the a-direction but have a noncollinear arrangement along the c-direction. Our density functional calculations for LiNaCo[PO_4]F show that the FM $Co2FO_3$ chains result from a strong intrachain FM exchange, but the FM $Co1FO_3$ chain from the strong AFM interchain exchange. The adjacent $Co1FO_3$ and $Co2FO_3$ chains have an AFM coupling along the a-direction but adopt a noncollinear spin arrangement along the c-direction due to the interchain spin conflict.

■ ASSOCIATED CONTENT

Supporting Information

Tables S1, S2 and S3 and Figures S1 and S2. This material is available free of charge via the Internet at http://pubs.acs.org.

■ AUTHOR INFORMATION

Corresponding Author

*E-mail: benyahia.hamdi@aist.go.jp (H.B.Y.); shikano.masahiro@aist.go.jp (M.S.).

Notes

The authors declare no competing financial interest.

■ ACKNOWLEDGMENTS

Part of this work was carried out in the Li-EAD Project of the New Energy and Industrial Technology Development Organization (NEDO) in Japan. We are grateful to Professor Qiang Xu and Dr. Peizhou Li for collecting the single crystal data. The work at NCSU was supported by the computing resources of the NERSC center and the HPC center of NCSU.

■ REFERENCES

(1) Chernova, N. A.; Nolis, G. M.; Omenya, F. O.; Zhou, H.; Li, Z.; Whittingham, M. S. *J. Mater. Chem.* **2011**, *21*, 9865 and the references cited therein.
(2) Gong, Z. L.; Li, Y. X.; He, G. N.; Li, J.; Yang, Y. *Electrochem. Solid-State Lett.* **2008**, *11*, A60.
(3) Okada, S.; Ueno, M.; Uebou, Y.; Yamaki, J. I. *J. Power Sources* **2005**, *146*, 565.
(4) Nagahama, M.; Hasegawa, N.; Okada, S. *J. Electrochem. Soc.* **2010**, *157*, A748.
(5) Recham, N.; Chotard, J. N.; Jumas, J. C.; Laffont, L.; Armand, M.; Tarascon, J. M. *Chem. Mater.* **2010**, *22*, 1142.
(6) Ramesh, T. N.; Lee, K. T.; Ellis, B. L.; Nazar, L. F. *Electrochem. Solid-State Lett.* **2010**, *13* (4), A43.
(7) Ellis, B. L.; Makahnouk, W. R. M.; Makimura, Y.; Toghill, K.; Nazar, L. F. *Nat. Mater.* **2007**, *6*, 749.
(8) Ellis, B. L.; Makahnouk, W. R. M.; Weetaluktuk, W. N. R.; Ryan, D. H.; Nazar, L. F. *Chem. Mater.* **2010**, *22*, 1059.
(9) Ben Yahia, H.; Shikano, M.; Tatsumi, K.; Koike, S.; Kobayashi, H. *Dalton Trans.* **2012**, *41*, 5838.
(10) Ben Yahia, H.; Shikano, M.; Sakaebe, H.; Koike, S.; Tabuchi, M.; Kobayashi, H.; Kawaji, H.; Avdeev, M.; Miiller, W.; Ling, C. D. *Dalton Trans.* **2012**, in press.
(11) Petricek, V.; Dusek, M.; Palatinus, L. JANA2006, *Structure Determination Software Programs*, Institute of Physics, University of Prague, Prague, Czech Republic, 2006.
(12) Rodriguez-Carvajal, J. *Physica B* **1993**, *192*, 55.
(13) (a) Kresse, G.; Hafner, J. *Phys. Rev. B* **1993**, *47*, 558. (b) Kresse, G.; Furthmüller, J. *Comput. Mater. Sci.* **1996**, *6*, 15. (c) Kresse, G.; Furthmüller, J. *Phys. Rev. B* **1996**, *54*, 11169.
(14) Perdew, J. P.; Burke, K.; Ernzerhof, M. *Phys. Rev. Lett.* **1996**, *77*, 3865.
(15) Dudarev, S. L.; Botton, G. A.; Savrasov, S. Y.; Humphreys, C. J.; Sutton, A. P. *Phys. Rev. B* **1998**, *57*, 1505.
(16) Dutreilh, M.; Chevalier, C.; El-Ghozzi, M.; Avignant, D.; Montel, J. M. *J. Solid State Chem.* **1999**, *142*, 1.
(17) Yakubovich, O. V.; Massa, W.; Kireev, V. V.; Urusov, V. S. *Dokl. Phys.* **2006**, *51*, 474.
(18) Brown, I. D.; Altermatt, D. *Acta Crystallogr., Sect. B: Struct. Sci.* **1985**, *B41*, 244.
(19) Brese, N. E.; O'Keefe, M. *Acta Crystallogr., Sect. B: Struct. Sci.* **1991**, *B47*, 192.
(20) Ben Ali, A.; Maisonneuve, V.; Kodjikian, S.; Smiri, L. S.; Leblanc, M. *Solid State Sci.* **2002**, *4*, 503.
(21) Shannon, R. D. *Acta Crystallogr., Sect. A: Cryst. Phys., Diffr., Theor. Gen. Crystallogr.* **1976**, *A32*, 751.
(22) Yahia, H. B.; Gaudin, E.; Darriet, J.; Banks, M.; Kremer, R. K.; Villesuzanne, A.; Whangbo, M. H. *Inorg. Chem.* **2005**, *44*, 3087.
(23) Ben Yahia, H.; Gaudin, E.; Boulahya, K.; Darriet, J.; Son, W. J.; Whangbo, M. H. *Inorg. Chem.* **2010**, *49*, 8578.
(24) Hammond, R.; Barbier, J. *Acta Crystallogr., Sect. B: Struct. Sci.* **1996**, *B52*, 440.

(25) Sanz, F.; Parada, C.; Ruíz-Valero, C. *J. Mater. Chem.* **2001**, *11*, 208.
(26) Mydosh, J. A. *Spin Glasses: An Experimental Introduction*; Taylor and Francis: London, 1993.
(27) Wong, P.; von Molnar, S.; Palstra, T. T. M.; Mydosh, J. A.; Yoshizawa, H.; Shapiro, S. M.; Ito, A. *Phys. Rev. Lett.* **1985**, *55*, 2043.
(28) (a) Greedan, J. E. *J. Mater. Chem.* **2001**, *11*, 37 and the references cited therein. (b) Dai, D.; Whangbo, M.-H. *J. Chem. Phys.* **2004**, *121*, 672.
(29) Whangbo, M.-H.; Koo, H.-J.; Dai., D. *J. Solid State Chem.* **2003**, *176*, 417.
(30) (a) Dai, D.; Whangbo, M.-H. *J. Chem. Phys.* **2001**, *114*, 2887. (b) Dai, D.; Whangbo, M.-H. *J. Chem. Phys.* **2003**, *118*, 29.
(31) Smart, J. S. *Effective Field Theory of Magnetism*; Saunders, Philadelphia, PA, 1966.

■ NOTE ADDED AFTER ASAP PUBLICATION

This paper was published on the Web on August 2, 2012, with minor text errors. The corrected version was reposted on August 6, 2012.